Acta Crystallographica Section D
Biological Crystallography
ISSN 0907-4449

Macromolecular crystallography with a third-generation synchrotron source

Peter F. Lindley

ESRF, BP-220, F-38043 Grenoble CEDEX, France

Correspondence e-mail: lindley@esrf.fr

Received 20 January 1999
Accepted 22 June 1999

The European Synchrotron Radiation Facility (ESRF) at Grenoble, France, is a 6 GeV machine producing hard X-radiation that can be used for pure and applied research in a wide range of disciplines including physics, chemistry, structural biology, materials science, the earth sciences, engineering and medicine. The overall nature of the machine will be described, including the features that give rise to the notation 'third-generation source'. The ESRF is equipped with a number of beamlines which can be used for macromolecular crystallography. Applications include the use of very small crystals, large unit cells, data collection at high resolution, anomalous dispersion measurements for phase determination and time-resolved studies. Key features of these applications will be described.

1. Introduction to the European Synchrotron Radiation Facility (ESRF)

1.1. Historical perspective

The original ideas for a high-energy European synchrotron-radiation facility arose in the mid-1970s and funding was eventually approved by the 12 member states in 1986. Construction was started in 1988 and the first electron beam was circulated within the storage ring in 1992. The user service began in 1994 and the construction phase, comprising 30 public beamlines, most of which are based on insertion devices, was completed at the end of 1998. In addition to the public beamlines, there are ten Collaborative Research Group (CRG) beamlines based on bending-magnet sources and funded by individual member states or consortia. It can therefore be seen that the ESRF project has taken some 20–25 years to move from conception to completion. However, it is pleasing to note that after funding was approved, this joint European project was completed on time, within budget and with certain important specifications that outperform the original design phase by at least a factor of two. In addition, certain key parameters, for example brilliance, are increased by an order of magnitude. The 12 member states involved in the founding of the ESRF (France, Germany, Italy, United Kingdom, Spain, Switzerland, Belgium, The Netherlands, Denmark, Finland, Norway and Sweden) have recently been joined by two associate members, Portugal (1998) and Israel (1999). It is hoped to attract further associate members and in this context the Czech Academy of Sciences has recently signed an interim agreement.

1.2. The main machine components of the ESRF

The ESRF essentially comprises of three main components. The pre-injector is a 16 m long linear accelerator (linac) which

produces electrons and accelerates them to an energy of 200 MeV. The booster synchrotron is a 10 Hz cycling synchrotron with a circumference of 300 m and increases the energy of the electrons to 6 GeV. In the main storage ring, which has a circumference of 844.4 m, bunches of electrons circulate at 6 GeV providing very intense X-rays at each passage inside the bending magnets or insertion devices (undulators or wigglers). The beam is guided onto the pseudo-circular orbit by 64 bending magnets and is focused by 320 quadrupole magnets. A further 224 sextupole magnets control the effect linked to the energy dispersion of the electrons (chromatic aberration). The storage-ring components are arranged in 16 super-period cells with the same magnet distribution (the Chasman–Green structure). Each super-period cell has two segments, a high- and a low-β (see below) segment, and each segment has one straight section (giving a total of 32) of 6 m in length, where insertion devices up to 5 m in length can be installed. As the electrons pass through the bending magnets and insertion devices they radiate photons, and radio-frequency cavities (352.2 MHz) are needed to restore the energy lost in this way and to maintain the energy at the nominal 6 GeV. The photon beams emerge tangentially to the various sources and can be used to pursue studies in a whole range of scientific disciplines including physics, chemistry, materials science, geophysics, engineering, environmental science, medicine and structural biology.

1.3. Synchrotron radiation from bending magnets

Synchrotron radiation is produced when electrons (or positrons) moving close to the speed of light are subjected to a magnetic field. The radiation is emitted in a continuous-wavelength spectrum around a characteristic wavelength λ_c (Å) which is inversely proportional to the square of the energy E (GeV) of the electron beam and to the field of the magnet B (T),

$$\lambda_c = 18.65/E^2B.$$

For an ESRF bending magnet with $B = 0.8$ T, then $\lambda_c = 0.65$ Å and this compares, for example, with 3.89 Å for the SRS (Daresbury Laboratory, UK) where $E = 2.0$ GeV and $B = 1.2$ T. The radiation is confined to a narrow cone with an opening angle of order $(1/\gamma) = mc^2/E$ (where m is the mass of an electron and c is the velocity of light). For a 6 GeV storage ring this angle is smaller than 20 arcsec (~80 µrad). The radiation is also polarized linearly in the orbit plane and elliptically outside the plane.

Some of the more important ESRF machine parameters from the user viewpoint are given in Table 1; the following definitions may clarify matters for non-synchrotron radiation specialists. The emittance (E_{xy}) is defined in essence as the product of the electron-beam size and its angular divergence and is normally given for both the horizontal and vertical directions of the electron beam; the coupling is defined as the ratio of the vertical to the horizontal emittance. A small emittance indicates that the corresponding X-ray beam is also small and highly collimated, therefore giving rise to a high brilliance. A small coupling means that if the horizontal brilliance is very high, the vertical brilliance will be even better because the vertical emittance will be decreased by the coupling factor. The β functions roughly define the electron-beam envelope all around the machine, and in the horizontal dimension alternate between low β and high β. More precisely, they are the amplitude functions defining the balance between the source dimensions and divergence at any point around the ring. The r.m.s. beam size (σ_{xy}) and the r.m.s. beam divergence (σ'_{xy}) are given by

Table 1
ESRF machine parameters.

(*a*) Electron-beam parameters.

Parameters	Direction	Values
Energy (GeV)		6.04
Current (mA)		200
Emittance (nm rad)	Horizontal	3.9
	Vertical	0.030 (0.8% coupling)
R.m.s. energy spread (%)		0.1
β for high β ID (m)	Horizontal	35.6
	Vertical	2.5
β for low β ID (m)	Horizontal	0.5
	Vertical	2.73
β for bending magnet (m)	Horizontal	2.2
	Vertical	34.9

(*b*) R.m.s. photon beam sizes and divergences.

Source	Direction	Electron beam	Undulator radiation (length 1.65 m)		
Photon energy (keV)			3	10	30
R.m.s. divergence (µrad)					
High β ID	Horizontal	10.5	15.3	12.1	11.0
	Vertical	3.9	11.9	7.3	5.3
Low β ID	Horizontal	88.3	89.0	88.5	88.4
	Vertical	3.8	11.8	7.2	5.2
Bending magnet	Horizontal	108.0			
	Vertical	1.1			
R.m.s. source size (µm)					
High β ID	Horizontal			395.0	
	Vertical			9.9	
Low β ID	Horizontal			57.0	
	Vertical			10.3	
Bending magnet	Horizontal			126.0	
	Vertical			36.9	

(*c*) Performance of the ESRF source in multi-bunch mode in 1998 compared with Foundation Phase design specifications.

Parameters	Routinely achieved in User Support Mode in 1998	Foundation Phase Report
Electron-beam current (mA)	200	100
Associated lifetime (h)	50	8
Lifetime at 100 mA (h)	80	8
Horizontal emittance, ε_H (m rad)	3.9×10^{-9}	6.8×10^{-9}
Vertical emittance, ε_V (m rad)	30×10^{-12}	620×10^{-12}
ID minimum gap (mm)	11	20
Brilliance at 1.0 Å for a 1.6 m undulator [photons s^{-1} mm^{-2} $mrad^{-2}$ (0.1% $\Delta\lambda/\lambda)^{-1}$]	4×10^{19} (low β_z), 3.37×10^{19} (high β_z)	6×10^{17}

$$\sigma_{xy} = (\beta_{xy} E_{xy})^{1/2},$$
$$\sigma'_{xy} = (E_{xy}/\beta_{xy})^{1/2}.$$

Machines such as the ESRF can be operated with very small values for the emittance and a coupling of less than 1%. Such small highly collimated sources give rise to very high brilliance, defined as the number of photons s^{-1} mm^{-2} $mrad^{-2}$ $(0.1\%\ \Delta\lambda/\lambda)^{-1}$.

1.4. Insertion devices (IDs)

IDs are comprised of an array of closely spaced magnets of opposite polarity which deflect the electrons by small amounts from a linear path, thus giving rise to synchrotron radiation at each position of deflection. The deflections are sinusoidal, so that the average path of the electrons through the ID remains linear. There are several types of IDs, as schematically indicated in Fig. 1. Wavelength shifters are characterized by a single and relatively wide deflection, producing a significant decrease in λ_c so that the radiation spectrum is shifted to higher energy. Multipole wigglers have somewhat smaller deflections and act as multiple sources for which the phase relationships are random, so that the total intensity is the sum of the intensities from the individual poles and the spectrum comprises a continuum of wavelengths. The source size and divergence is comparable with that of a normal bending magnet. In an undulator, the deflection is kept within the natural angle of emission $(1/\gamma)$, so that the radiation from the different poles is 'in-phase' for a particular energy (and therefore wavelength); the net intensity is then the sum of the squares of the individual amplitudes. Undulators therefore produce the X-ray sources with the highest brilliance. In general, the divergence of the undulator radiation depends on the undulator length, photon energy, electron energy spread and the undulator tuning. The tuning of the undulator corresponds to a maximum of the spectral flux per unit surface, on-axis of the electron beam. There exists one such maximum for each odd harmonic of the spectrum. Tuning the photon energy to higher (lower) values or equivalently tuning the magnetic gap to lower (higher) values may result in a narrower (wider) divergence. In the limit of very small gaps between the magnetic poles and equivalent very high magnetic fields, an undulator becomes a wiggler and the radiation is no longer as collimated (see Fig. 1*b*). The minimum magnetic gap that can be achieved in a given machine is determined by the degradation that it imposes on the lifetime of the electron beam.

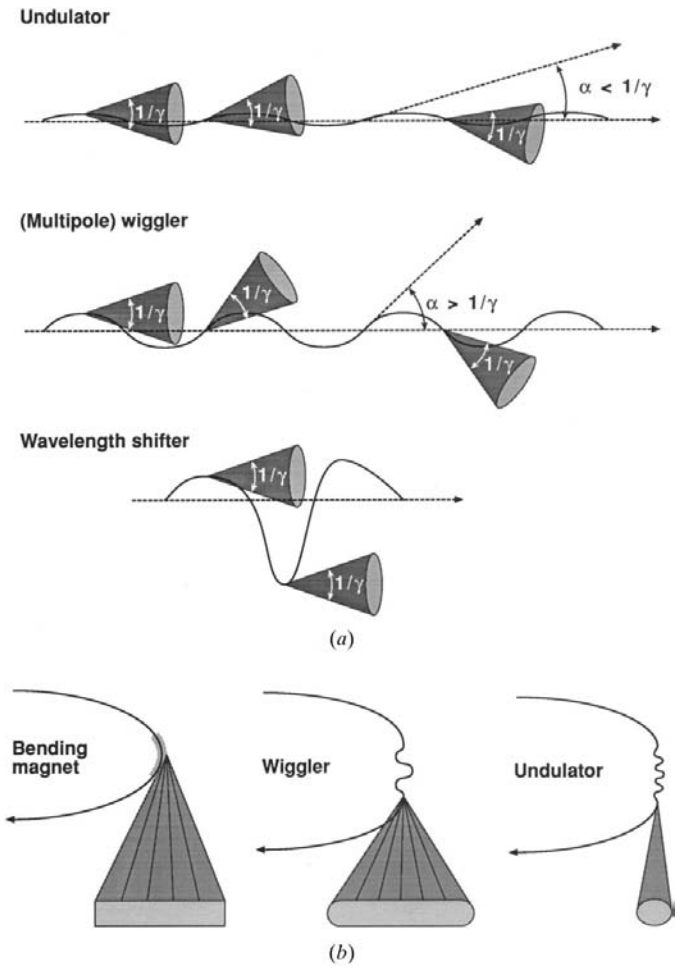

Figure 1
Insertion devices (IDs). (*a*) The various types of insertion device. Most insertion devices present a periodic sinusoidal magnetic field. They are then called multipole 'wigglers' or 'undulators' depending on the so-called deflection (or magnetic field) parameter K; $K = \alpha\gamma = B_0\lambda$, where α is the maximum deflection angle; B_0, the maximum field strength, is in T and λ is in m. (*b*) Beam shapes generated by insertion devices.

The 6 m straight sections at ESRF can accommodate up to three 1.6 m long ID units with a minimum gap between the magnet poles of 11 mm. The use of up to three individual ID units rather than one 5 m unit enables an important flexibility in the choice of a radiation source so that it can be readily matched to the requirements of a particular experiment. There is also considerable saving in capital cost and maintenance compared with a single ID 5 m in length. Currently the brilliance obtainable from a 1.6 m undulator is approaching 10^{20} photons s^{-1} mm^{-2} $mrad^{-2}$ $(0.1\%\ \Delta\lambda/\lambda)^{-1}$. This can be compared with the calculated diffraction limit (the maximum photon brilliance theoretically achievable at zero emittance) of about 10^{23} at 200 mA current and for λ = 1.0 Å. The ESRF and other third-generation sources (the 7 GeV APS at Argonne National Laboratory, Chicago, USA, and the 8 GeV SPring8 machine in Japan) are therefore working close to their theoretical limits. To achieve a brilliance significantly above the current values will presumably be the task of the fourth-generation machines based on free-electron laser technology.

1.5. Characteristics of beam modes at the ESRF

Owing to the radio-frequency accelerating cavities, which compensate for the energy loss by synchrotron radiation, the electrons travel around the ring in bunches. The minimum 3 ns time separation between two successive bunches corresponds to the radio-frequency period. The bunches are positioned at a very precise phase with respect to the radio-frequency field to maintain the acceleration each time they cross the accelerating cavities. In the time coordinate, each bunch has a duration of around 150 ps. The bunches of electrons (each of diameter

Table 2
ESRF beamlines concerned with macromolecular crystallography (MX).

The table does not include various Collaborative Research Group beamlines which can be used for MX and for which the ESRF has a one-third usage.

Beamline	Time dedicated to MX (%)	Specific applications	Detectors
ID2†	50	Monochromatic data collection, large unit cells	IP
ID9	30	Time-resolved Laue studies	CCD, IP
ID13	30	Micro-focus, small crystals	CCD, IP
ID14		Quadriga – principal MX workhorse	
EH1‡	100	Monochromatic	CCD
EH2	100	Monochromatic	CCD
EH3	100	Large proteins and viruses, limited tuneability	CCD, IP§
EH4	100	Multiwavelength anomalous diffraction (MAD) and monochromatic data collection; very high brilliance	CCD
BM14¶	100	MAD	CCD, IP
ID29	100	MAD; due for completion in 2000	CCD, IP

† The use of ID2 for MX work will be gradually phased out during 1999/2000. ‡ Experimental hutch EH1 will not be complete until June 1999. § EH3 is equipped with a large robot-controlled off-line image-plate detector system. ¶ This beamline derives its radiation from a bending-magnet source and is being transferred to ID29.

about 300 µm and length 6 mm) circulate around the 844 m storage ring some 350 000 times per second. Although the ESRF storage ring could theoretically accommodate some 900 electron bunches, the most common mode is the 2 × 1/3rd fill. In this mode, the storage ring contains two groups of 300 equally spaced bunches which at any given point in time occupy one-third of the circuit, and these groups are separated by one-sixth of the circuit which is left empty. This enables a circulating ring current of 200 mA and re-injection (every 12 h, when the ring current has typically decayed to 150 mA) takes only a few minutes. However, many other bunch-mode structures are possible, including 16 equally spaced bunches, hybrid modes with a one-third fill and the remainder empty or filled with between one and four equally spaced single bunches, and the single bunch mode. In the single-bunch mode, the maximum current is some 16 mA and the need to have a bunch purity of better than 10^{-7} (very low contamination of adjacent bunches) normally necessitates a rather long 'cleaning' procedure during a new injection, which can take up to 20 min. In addition to the low current, the lifetime in the single-bunch mode is only a few hours; however, this mode is very useful for time-resolution studies.

1.6. Summary of the main features of a third-generation synchrotron source

In summary, the ESRF is a 6 GeV machine equipped with insertion devices capable of producing high-energy X-rays with full tuneability of the X-ray energy, low emittance of the electron beam, high brilliance and high natural collimation. In addition, the small source size can give a significant degree of transverse coherence, *i.e.* at the object the X-rays are practically in the form of a plane wave (temporal coherence is obtained using monochromators which can give a high degree of monochromaticity) and this characteristic opens up many new possibilities with respect to X-ray imaging techniques. Further information can be obtained by consulting the ESRF WWW pages (http://www.esrf.fr/machine/machine.html).

2. Macromolecular crystallography

2.1. Introduction

The source characteristics of the ESRF are ideally matched to a number of difficult problems in macromolecular crystallography. The high brilliance and high degree of collimation allow intensity data to be collected from small weakly diffracting crystals, whilst the wavelength tuneability readily enables the technique of multiple-wavelength anomalous dispersion to be used for phase determination over a wide range of absorption edges. Macromolecular crystallography at the ESRF is handled by a number of different beamlines, but the principal ones are shown in Table 2. In this section, only some of the beamlines will be described; further details can be obtained at http://www.esrf.fr/exp_facilities/blhb.htm.

2.2. High-resolution data collection – beamline ID14

The Quadriga beamline ID14 (Wakatsuki *et al.*, 1998) is designed to have four simultaneously operating stations: an end station EH4 equipped with a fast-scan double-crystal monochromator and three side stations EH1–3 deriving their radiation through the use of thin diamond crystals. Two undulators, each with a length of 1.65 m and minimum achievable gap of 16 mm, provide the high-brilliance X-ray source. The first undulator, with a periodicity of 42 mm, is tuneable over a wide wavelength range (7–35 keV), whereas the second, with a periodicity of 23 mm, is a single line undulator with very little tuneability but optimized to give high brilliance around 13.5 keV (0.92 Å). The second undulator induces only a small heat load on the optical components and is operated in tandem with the first; an option exists to add a third undulator to enhance the high brilliance at around 12.7 keV (0.979 Å), the Se $K\alpha$ edge.

Fig. 2 shows schematically the overall layout of the Quadriga beamline, and details of the beamline optical components and detectors are summarized in Table 3. The end station, EH4, is equipped with a fast-scanning Kohzu double-crystal monochromator for which the first element has to be cooled with liquid nitrogen. The beam is then focused with an uncooled toroidal mirror, 80 cm in length and coated with rhodium in order to avoid absorption edges in the energy range 10–15 keV. The focus achievable at the sample is around 0.5 × 0.4 mm. For the side stations, EH1–3, the diamond crystals use the (111) reflection, either in the Bragg mode (60 µm thickness) or the Laue mode (150 µm thickness).

Table 3
Quadriga beamline ID14: beamline optical components and detectors.

	Monochromator	Focusing	Energy ranges (keV)	Wavelength (Å)
EH1	Diamond(111)	Sagitally focusing Ge(220) + ML†	∼13.3	∼0.93
EH2	Diamond(111)	Toroidal mirror	∼13.3	∼0.93
EH3	Diamond(111)	Sagitally focusing Ge(220) + ML†	8.6–13.9	1.44–0.89
EH4	Double-crystal Si(111) or Si(311)	Toroidal mirror	7.3–35.4	1.70–0.35

† ML, multilayer device.

Subsequently, the beam is brought back into the parallel position using either a sagitally bent Ge(220) crystal for vertical focusing and a bent multilayer component for focusing in the horizontal direction and rejection of higher harmonics, or a flat Ge(220) crystal with further focusing achieved with a toroidal mirror. For EH3, the multilayer comprises a silicon substrate on a bimorph piezoelectric ceramic material. The substrate is coated with 100 layers of ruthenium and boron carbide with a d spacing of 68 Å, and the device has a reflectivity of greater than 65% at 13.5 keV. The multilayer is bent by applying a high voltage to the bimorph material. Station EH3 is tuneable between 8.2 and 13.8 keV; this is achieved by translating the Ge crystal and the multilayer. However, caution has to be exercised to avoid interference with EH4.

Stations EH1 and EH2 are currently equipped with single-axis φ-spindle goniometers and CCD detectors (MAR Research 133 or 165 mm diameter). Station EH3 is equipped with a four-circle κ diffractometer with a horizontal ω axis and a 2θ arm holding a MAR Research 133 mm CCD camera. This is the normal configuration, but larger unit cells can also be accommodated using a flat plate off-line image-plate device utilizing Weissenberg geometry. This camera can hold up to two 40 × 80 cm plates, thus forming a maximum active area of 8000 × 8000 pixels. A robot can be programmed to coordinate the loading and unloading of up to 16 plates in conjunction with a given set of oscillation ranges. The camera can be translated perpendicular to the X-ray beam and with a knowledge of the crystal lattice type, the unit-cell dimensions and the crystal orientation, optimum coupling constants between the Weissenberg translation and the spindle axis and oscillation range are calculated to minimize overlapping of reflections. A special off-line cylindrical drum scanner has been constructed to read the image plates (Cipriani *et al.*, 1997).

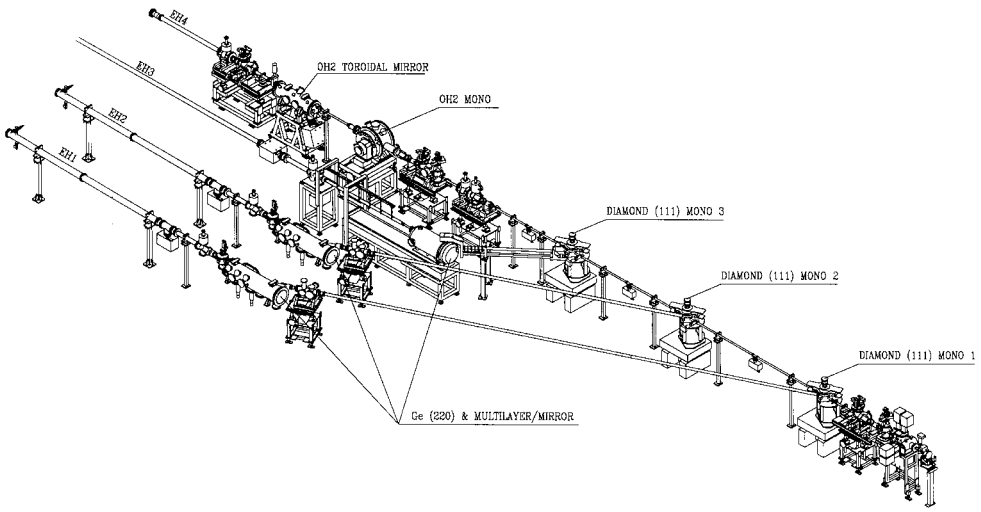

Figure 2
A schematic view of the Quadriga beamline ID14 at the ESRF. (Reproduced with permission from the *Journal of Synchrotron Radiation*.)

Table 4
Quadriga beamline ID14-3: example of a partial data set collected with the off-line image-plate system using pseudo-Weissenberg geometry.

Tropinone reductase II (S. Wakatsuki, personal communication). Space group $P6_122$ with $a = 88.59$, $c = 338.34$ Å. Data were collected to a resolution of 1.2 Å using 2.0° oscillations and 45 s exposures; 30° of data (15 images). The c axis was aligned almost parallel to the spindle axis permitting 2.0° oscillations. The wavelength was 0.93 Å and a crystal-to-detector distance of 409 mm was used. (Partial reflections are not included.)

Resolution (Å)	N_{hkl}	$I/\sigma(I)$	Completeness† (%)	Multiplicity	R_{sym}‡
3.79	5174	25.1	64.7	2.4	0.025
2.68	12846	24.6	91.6	3.0	0.026
2.19	17363	22.8	97.0	3.1	0.028
1.90	19554	17.4	93.2	2.8	0.034
1.70	18974	13.6	80.5	2.6	0.050
1.55	17381	9.7	67.1	2.6	0.076
1.43	15918	6.2	56.8	2.6	0.123
1.34	15488	3.6	51.8	2.6	0.212
1.26	15690	2.4	49.4	2.5	0.327
1.20	14014	1.9	41.9	1.7	0.404
Overall	152402	14.7	65.0	2.6	0.040

† A single 40 × 80 cm image plate was used for each oscillation. The shorter edge of the image plate significantly affected the completeness of the data beyond a resolution of 2.1 Å. This resolution on the plate corresponds to 20 cm from the X-ray beam with a crystal-to-plate distance of 409 mm and a wavelength of 0.93 Å. ‡ $R_{sym} = \sum[(I - \langle I\rangle)^2 / \sum I^2]$.

Station EH4 is also equipped with a single-axis φ-spindle goniometer, but the detector is an Area Detector Systems Corporation Quantum 4, 2 × 2 CCD detector mounted on a pseudo-2θ arm. The arm comprises a translation stage, 1 m in length, on which vertical translation and tilt stages are mounted to simulate 2θ motion.

All Quadriga stations are fitted with Oxford Cryosystems Cryostream liquid-nitrogen sample-cooling devices.

Tables 4 and 5 show particular examples of the data which have been collected on the Quadriga beamline using the off-line image-plate detector system on station EH3 and the ADSC Quantum 4 detector on station

Table 5
Quadriga beamline ID14-4: the ADSC Quantum 4 detector system.

(*a*) Data collection for a very small weakly diffracting crystal with a large unit cell.

Cytochrome bc_1 complex from bovine heart (S. Iwata, personal communication). Space group $P6_5$ with a = 130.1, c = 720.9 Å. The asymmetric contains a dimer, 490 kDa, and the solvent content is around 65%. The crystals grew as needles with dimensions 0.03 × 0.05 × 0.30 mm. Data were collected to a resolution of 2.5 Å using 0.3° oscillations and 10 s exposures; 60° of data (200 images) required about 1 h. The wavelength was 0.93 Å and a crystal-to-detector distance of 240 mm was used. Note that this data set is really working at the limit of the Quantum 4 detector in terms of reflection separation and represents an excellent achievement for a CCD-based detector. The relatively high values of R_{sym} and the deviation of the χ^2 values from unity arise, at least in part, from the necessity of choosing a very small mask to ensure the separation of the reflections. Such a procedure is not recommended for routine data collection. The effective resolution is around 3.1 Å, based on the criteria that R_{sym} should be ≤20% and $I/\sigma(I)$ should be >3.0.

Resolution range (Å)	N_{hkl}	$\langle I \rangle$	$I/\sigma(I)$	χ^2†	R_{sym}‡
40.00–5.00	27477	2370.8	14.9	1.566	0.073
5.00–3.97	27732	1724.3	15.1	1.759	0.078
3.97–3.47	27762	957.9	10.0	1.540	0.101
3.47–3.15	27470	469.3	4.9	1.215	0.157
3.15–2.92	26852	276.5	2.6	1.016	0.212
2.92–2.75	26351	194.2	1.7	0.906	0.265
2.75–2.61	25930	166.0	1.3	0.848	0.314
2.61–.50	24767	162.6	1.2	0.874	0.345
Overall	214341	807.5	6.9	1.314	0.094

(*b*) A typical example of 'fast' data collection from crystals of an acetylcholinesterase complex (R. Ravelli, EMBL Grenoble Outstation, personal communication).

Space group $P3_121$ with a = 111.98 and c = 137.78 Å. The asymmetric unit has a molecular weight of 54 kDa and the solvent content is around 68%. The crystal size was 0.1 × 0.1 × 0.08 mm. Data were collected to a nominal resolution of 2.0 Å using 0.5° oscillations and 1 s exposures; 30° of data, with a total exposure time of 60 s. The wavelength was 0.932 Å and a crystal-to-detector distance of 175 mm was used. A total of 119 775 measurements yielded 66037 unique reflections (97.3% completeness), with a total data-collection time of 724 s. The values of $I/\sigma(I)$ and R_{sym} indicate that the effective resolution is about 2.15 Å.

Resolution range (Å)	N_{unique}	$\langle I \rangle$	$I/\sigma(I)$	χ^2†	R_{sym}‡
30.00–4.31	6469	6345.5	16.3	1.158	0.048
3.42–2.99	6796	1993.4	15.5	1.214	0.065
2.99–2.71	6744	961.8	11.8	1.092	0.077
2.71–2.52	6699	581.6	8.4	1.087	0.080
2.52–2.37	6687	438.2	6.0	0.980	0.092
2.37–2.25	6663	407.0	4.7	1.275	0.164
2.25–2.15	6353	290.2	3.1	1.086	0.196
2.15–2.07	6640	204.1	2.2	0.882	0.205
2.07–2.00	6607	149.6	1.6	0.800	0.255
Overall	66037	1642.8	11.6	1.060	0.061

† $\chi^2 = \sum\{(I - \langle I \rangle)^2/[\text{error}^2 \times N/(N-1)]\}$. ‡ $R_{sym} = \sum[(I - \langle I \rangle)^2/\sum I^2]$.

EH4, respectively. They are not meant to demonstrate the quality of routine data collection at the ESRF using, for example, an optimized data-collection strategy, but rather show what can be achieved in extreme circumstances. Thus, the data set collected with the ADSC for an alternative crystal form of the cytochrome bc_1 complex (Iwata *et al.*, 1998) shows the versatility of this detector with respect to very small weakly diffracting crystals with large unit cells (the c unit-cell dimension exceeds 700 Å), although it is clear that an image-plate system would lead to improved data quality in this particular case. The 'fast' data collection for the acetylcholinesterase complex demonstrates what can be achieved, for example, in the case where radiation damage necessitates minimization of the data-collection time.

2.3. A microfocus beamline for very small crystals – beamline ID13

The ID13 beamline has been specifically designed to study micr-diffraction and other microapplications. The source is an undulator with a periodicity of 46 mm giving a source size of 0.133 mm horizontal × 0.109 mm vertical (full-width half-maximum) and respective divergences of 0.233 × 0.043 mrad; the unfocused beam size at 30 m from the source is therefore 7.1 × 1.4 mm. For microdiffraction purposes (see Fig. 3), the optical components comprise a channel-cut Si(111) monochromator with liquid-nitrogen cooling of the first element and an ellipsoidal mirror. The mirror is designed to demagnify the source by a factor of ten, but mirror aberrations increase the focal-spot size. Currently a focal spot of approximately 20 µm horizontally and 40 µm vertically has been reached. Post-collimation with capillary optics can yield a 7 µm (full-width half-maximum) focal spot at the sample position, with an X-ray flux of some 2×10^{11} photons s^{-1} at an energy of 13 keV. However, there is a price to pay and this is in the form of a compromise between optimizing the flux density at the sample and having an increased divergence of the diffracted beams, as indicated in Fig. 4(*b*). In practice, this means that if a crystal has a large unit-cell dimension, care has to be taken in orientating the crystal with respect to the beam.

Beamline ID13 has been used extensively for data collection from very small crystals; Fig. 4 shows diffraction patterns taken from bacteriorhodopsin and the H50S ribosome particle. In the case of bacteriorhodopsin, the crystals were very thin (5 µm) plates with typical plate cross sections of up to 40 µm, grown by the cubic lipidic phase method (Pebay-Peyroula *et al.*, 1997). The H50S ribosome particle diffraction pattern (Yonath *et al.*, 1998) clearly shows the effect of the horizontal divergence resulting from the micro-focus optical system.

2.4. Time-resolved studies – beamline ID9

ID9 is a white-beam station designed both for time-resolved experiments in macromolecular crystallography and chemistry, and for high-pressure studies. The beamline is served by three IDs: a 43-pole broad-band wiggler with a 70 mm period, a 71-pole undulator with a 46 mm period and a 129-pole mono-harmonic undulator with a 26 mm period. The white beam can be focused by a tuneable toroidal mirror and delivered to one of three experimental tables covering the energy ranges 7–22, 7–30 and 7–40 keV, respectively. Complete details of the station optics can be obtained from http://www.esrf.fr/exp_facilities/ID9/handbook/.

A number of time-resolved methods designed to observe the structural changes undergone by macromolecules whilst carrying out their biological function have been developed at the ESRF (ESRF, 1996/1997; Bourgeois *et al.*, 1996; Srajer *et*

al., 1996). Myoglobin (Mb), a muscle protein which stores oxygen, has provided a useful test case. When Sir John Kendrew determined the structure of myoglobin in 1960, it immediately posed a problem, since it appeared from space-filling rigid models that there was no obvious way for oxygen to get in and out of the haem binding site. Clearly, a dynamic protein structure with channels opening and closing to permit access to and from the active binding site is a far more realistic model, but the location of these channels, the speed at which the ligand moves through them and the response time of the protein structure to ligand binding and dissociation posed interesting questions which could only be addressed by time-resolved methods. To this end, a team of scientists led by Keith Moffat (University of Chicago) and Michael Wulff (ESRF) triggered the dissociation of CO from a MbCO crystal with a 10 ns optical pulse and measured Laue diffraction patterns with 150 ps polychromatic X-ray pulses. CO was used as a surrogate for O_2 as it is easier to photo-detach from Mb and as it rebinds more slowly. Structures were determined at various times controlled by the time interval between the photolysis and the X-ray pulses. The intensity of the X-ray pulse was sufficient to record a Laue pattern with a single shot, making it possible to accumulate a complete set of Laue patterns at a sequence of times with a single MbCO crystal. An examination of the differences between these Laue patterns and that of the native Mb crystal has enabled a dissociation/association pathway to be defined. After 4 ns, an intermediate state is formed in which the CO is rotated by 90° and displaced some 4 Å from the Fe, within the haem pocket. This configuration lasts for around 350 ns and the function of this 'docking site' is to prevent the CO from recoiling back to the chemically attractive Fe. 1 µs after the optical pulse, the CO has left the pocket. In this time regime, the CO diffuses about in the outer protein for a fraction of a millisecond. It eventually recombines with an Fe atom through random collisions with the fluctuating haem and this recombination closes the photocycle. The time evolution of these features showed for the first time how the protein responds structurally to ligand dissociation and rebinding under ambient temperature conditions. The time resolution of the technique has now been improved down to an X-ray pulse length of around 100 ps by the use of a femtosecond laser. This new technique can be extended to many other photobiological systems such as bacteriorhodopsin, photoactive yellow protein and the photosynthetic reaction centre.

2.5. Multi-wavelength anomalous dispersion – beamline BM14

BM14 has an optical design suited to the rapid and accurate change of wavelength required by the multi-wavelength anomalous dispersion technique. The radiation source is a bending magnet, since at the time of conception of the beamline it was not clear that the maximum undulator energy (in the fundamental) could be extended beyond 14.4 keV (ESRF, 1987). (Now that it is well known that IDs can be readily used beyond this limit, a movement of the beamline to an ID source, ID29, is under way and is scheduled for completion in 2000.)

The general layout of the beamline is shown in Fig. 5. The first element, some 25.5 m from the source, is a pre-collimating rhodium-coated mirror of length 1.2 m with a grazing angle of 2.8 mrad and an acceptance of 0.11 mrad. This is followed at 27.5 m from the source by a Si(111) channel-cut monochromator, suitable for fast tuneability of the wavelength. Finally, focusing in the horizontal and vertical planes is achieved with a rhodium-coated toroidal mirror sited some 30.0 m from the source. Such an optical system can give an intensity of the order of 10^{12} photons s^{-1} integrated both vertically and horizontally/0.01% band pass (band pass is defined as $\Delta\lambda/\lambda$). The band pass for the monochromator is 1.9 $\times$ 10^{-4} and the useful wavelength range is between 0.6 and 2.0 Å; the focal-spot size at the sample, some 60 m from the source, is 0.4 $\times$ 0.8 mm maximum. Crystals can be mounted on a three-circle goniostat so that they can be oriented for an efficient collection of Friedel pairs of reflections, and cryo-cooling to liquid temperatures is available. The current detectors include a 133 mm diameter MAR Research CCD system and a 34.5 cm MAR Research on-line image-plate system.

MAD measurements on beamline BM14 can be undertaken 'routinely', although it should be stressed that care is required to ensure a good precision of the relatively weak anomalous signals. During 1998, when some 25 weeks of beam time were available with the ESRF operating in the two-thirds fill mode, a number of successful phasing experiments were undertaken involving Fe, Hg, Yb, Br, W, Pt, Au and Se; experiments involving selenomethionine derivatives accounted for roughly 60% of the total. The production of over 30 interpretable electron-density syntheses was reported to the ESRF scientists by users, whilst several more data sets are still at the

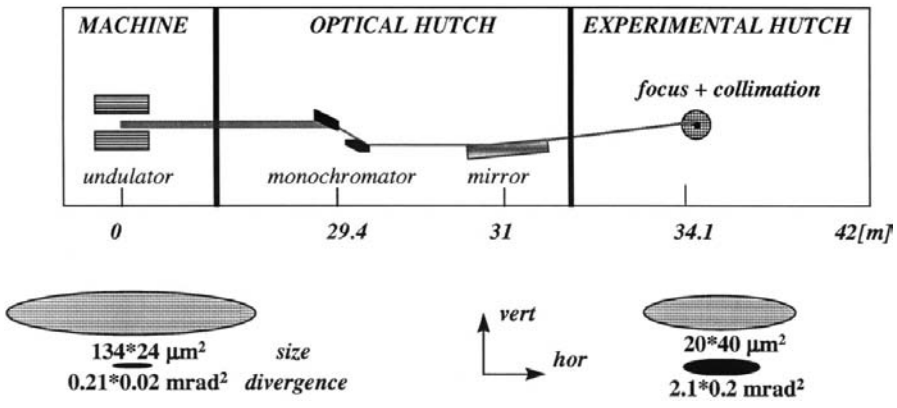

Figure 3
A schematic layout of the microfocus beamline ID13 at the ESRF.

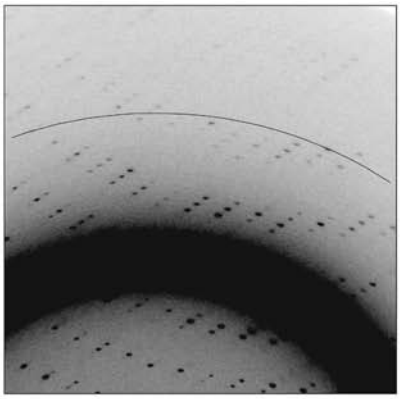

(*a*)

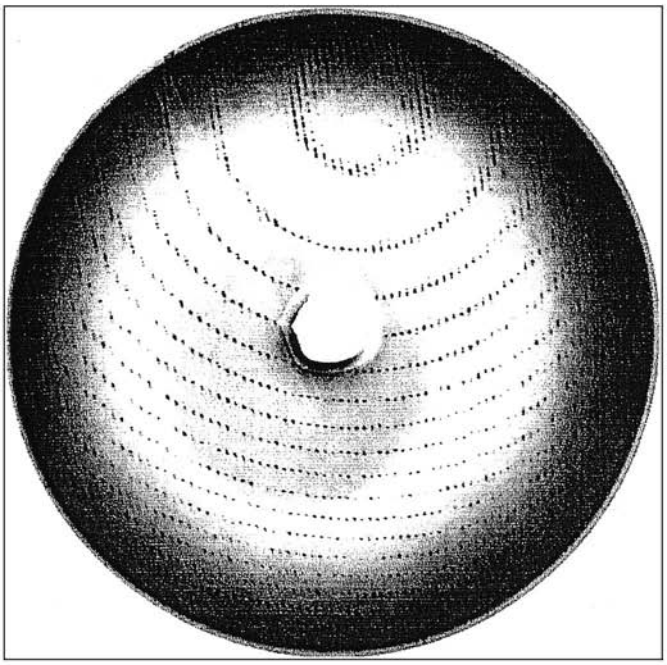

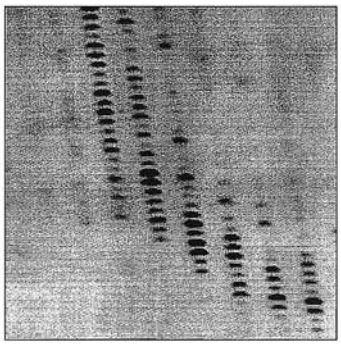

H50S Ribosome
A. Yonath *et al.*

space group	$C222_1$
unit cell	210 × 300 × 581 Å
crystal	180 × 140 × 50 µm
oscillation range	0.5°
pixel size	150 µm
sample–detector	657 mm

300 mm φ MAR-IP at 15.86 keV
3.5 Å at edge (3.2 reached)

(*b*)

Figure 4
Diffraction patterns taken on the microfocus beamline ID13. (*a*) Part of the diffraction pattern from a crystal of bacteriorhodopsin, unit-cell parameters $a = b = 62$, $c = 104$ Å. The unit-cell c axis can be clearly visualized running from bottom left to top right in the figure. The edge of the diffraction pattern represents a resolution of around 2.5 Å. Data along the c axis are difficult to obtain using cryo-electron microscopy techniques with two-dimensional crystals. (*b*) Diffraction patterns of the H50S ribosome complex. The inset diagram shows how the horizontal divergence of the microfocus beam causes the diffraction spot shape to elongate in the horizontal direction, thus necessitating careful mounting of the crystal. (Figure reproduced by courtesy of Professor Ada Yonath.)

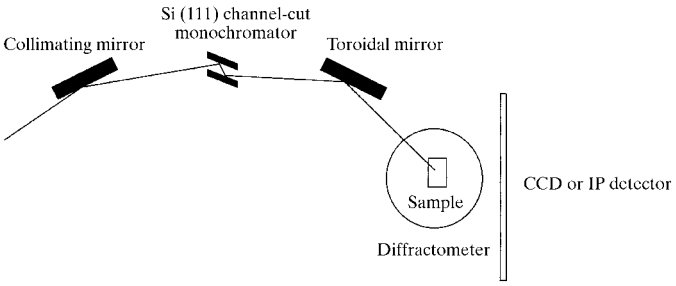

Figure 5
Schematic layout of beamline BM14.

processing stage. In optimum cases, the time taken from mounting the crystal specimen to obtaining an interpretable electron-density map was of the order of a few hours, and this can be expected to decrease in the medium-term future. Clearly, the MAD technique will continue to play a key role in *ab initio* macromolecular structure determination.

3. Summary

Various beamlines at the ESRF have been designed to use the full potential of a third-generation synchrotron source for macromolecular crystallography. The highly collimated high-brilliance X-ray beams attainable with insertion devices enable useful diffraction data to be collected from very small crystals and from weakly diffracting crystals with large unit cells. The time structure of the electron bunches enables time-resolved studies of the dynamic motion of biological macromolecules as they undergo their biological function.

The author gratefully acknowledges the assistance of the ESRF machine personnel (Director, Jean-Marc Filhol), the scientific secretary of the Experimental Division (Fabio Comin) and the staff who operate the ESRF/EMBL Joint Structural Biology Programme. In particular, he would like to thank Soichi Wakatsuki, Sean McSweeney, Raimond Ravelli, Wim Burmeister, Edward Mitchell and Hassan Belrhali (ID14), Michael Wulff (ID9), Christian Riekel and Manfred Burghammer (ID13), and Andrew Thompson and Gordon Leonard (BM14).

References

Bourgeois, D., Ursby, T., Wulff, M., Pradervand, C., Legrand, A., Schildkamp, W., Labouré, S., Srajer, V., Teng, T. Y., Roth, M. & Moffat, K. (1996). *J. Synchrotron Rad.* **3**, 65–74.
Cipriani, F., Casragna, J.-C., Claustre, L., Blampey, H., Wilkinson, C., Tomizaki, T., Burmeister, W. P. & Wakatsuki, S. (1997). *ESRF Newslett.* **28**, 30–32.
ESRF (1987). *ESRF Foundation Phase Report*, ch. 1, p. 41. BP-220, F-38043 Grenoble CEDEX, France,
ESRF (1996/1997). *ESRF Highlights*, pp. 69–72. BP-220, F-38043 Grenoble CEDEX, France.
Iwata, S., Lee, J. W., Okada, K., Lee, J. K., Iwata, M., Rasmussen, B., Link, T. A., Ramaswamy, S. & Jap, B. K. (1998). *Science*, **281**, 64–71.
Pebay-Peyroula, E., Rummel, G., Rosenbusch, J. P. & Landau, E. (1997). *Science*, **277**, 1676–1681.

Srajer, V., Teng, T., Ursby, T., Pradervand, C., Ren, Z., Adachi, S., Schildkamp, W., Bourgeois, D., Wulff, M. & Moffat, K. (1996). *Science*, **274**, 1726–1729.

Wakatsuki, S., Belrhali, H., Mitchell, E. P., Burmeister, W. P., McSweeney, S. M., Kahn, R., Bourgeois, D., Yao, M., Tomizaki, T. & Theveneau, P. (1998). *J. Synchrotron Rad.* **5**, 215–221.

Yonath, A., Harms, J., Hansen, H. A. S., Bashan, A., Schlünzen, F., Levin, I., Koelln, I., Tocilj, A., Agmon, I., Peretz, M., Bartels, H., Bennett, W. S., Krumbholz, S., Janell, D., Weinstein, S., Auerbach, T., Avila, H., Piolleti, M., Morlang, S. & Franceschi, F. (1998). *Acta Cryst.* A**54**, 945–955.